Am J Nucl Med Mol Imaging 2024;14(5):306-315
www.ajnmmi.us /ISSN:2160-8407/ajnmmi0158664

Original Article

Radiosynthesis and preclinical evaluation of a carbon-11 labeled PET ligand for imaging metabotropic glutamate receptor 7

Yinlong Li[1,2*], Zhiwei Xiao[1,2*], Wakana Mori[3*], Jiyun Sun[2], Tomoteru Yamasaki[3], Jian Rong[1,2], Masayuki Fujinaga[3], Jiahui Chen[1,2], Katsushi Kumata[3], Chunyu Zhao[1,2], Yiding Zhang[3], Thomas L Collier[1,2], Kuan Hu[3], Lin Xie[3], Xin Zhou[1], Wei Zhang[1], Zhendong Song[1], Yabiao Gao[1], Zhenkun Sun[6], Kuo Zhang[1], Jimmy S Patel[1,4], Chongzhao Ran[5], Ahmad Chaudhary[1], Douglas J Sheffler[7], Nicholas DP Cosford[7], Linqi Zhang[1], Chuangyan Zhai[1], Ahmed Haider[1,2], Hongjie Yuan[6], Ming-Rong Zhang[3], Steven H Liang[1,2]

[1]Department of Radiology and Imaging Sciences, Emory University, Atlanta, GA 30322, USA; [2]Division of Nuclear Medicine and Molecular Imaging, Massachusetts General Hospital & Department of Radiology, Harvard Medical School, Boston, MA 02114, USA; [3]Department of Advanced Nuclear Medicine Sciences, Institute for Quantum Medical Sciences, National Institutes for Quantum Science and Technology, Chiba 263-8555, Japan; [4]Department of Radiation Oncology, Winship Cancer Institute of Emory University, Atlanta, GA 30322, USA; [5]Athinoula A. Martinos Center for Biomedical Imaging, Department of Radiology, Massachusetts General Hospital and Harvard Medical School, Boston, MA 02114, USA; [6]Department of Pharmacology and Chemical Biology, Emory University School of Medicine, Atlanta, GA 30322, USA; [7]Cancer Molecular Therapeutics Program and Conrad Prebys Center for Chemical Genomics, Sanford-Burnham Prebys Medical Discovery Institute, La Jolla, CA 92037, USA. [*]Equal contributors.

Received June 22, 2024; Accepted August 29, 2024; Epub October 15, 2024; Published October 30, 2024

Abstract: Metabotropic glutamate receptor 7 ($mGlu_7$) is a G protein-coupled receptor that is preferentially found in the active zone of neurotransmitter release in the central nervous system (CNS). $mGlu_7$ plays a vital role in memory, learning, and neuronal development, rendering it a potential target for treating epilepsy, depression, and anxiety. The development of noninvasive imaging ligands targeting $mGlu_7$ could help elucidate the functional significance of $mGlu_7$ and accelerate drug discovery for neurological and psychiatric disorders. In this report, a novel carbon-11 labeled positron emission tomography (PET) tracer designated [^{11}C]18 (codenamed MG7-2109) was synthesized *via* ^{11}C-methylation in 23% decay-corrected radiochemical yield (RCY). *In vitro* serum stability, serum protein binding, *in vitro* autoradiography and *ex vivo* biodistribution studies of [^{11}C]18 were conducted. Preliminary PET imaging results revealed a homogeneous distribution of [^{11}C]18 and rapid clearance in rodent brains. This study provides valuable insights into the development of $mGlu_7$-targeted PET tracer based on an isoxazolo(5,4-c)pyridine scaffold.

Keywords: $mGlu_7$, negative allosteric modulator, positron emission tomography, radioligand

Introduction

Glutamate is the primary excitatory neurotransmitter in the mammalian central nervous system (CNS), orchestrating physiological processes involved in memory formation, synaptic plasticity, and neurodevelopment. Depending on their structures and physiological functions, two classes of glutamate receptors are identified as metabotropic glutamate receptors (mGlus) and ionotropic glutamate receptors (iGlus) [1]. iGlus are ligand-gated ion channels that regulate the excitatory neurotransmission rapidly, whereas mGlus are G protein-coupled receptors modulating signal transduction cascades, including the second messengers, ion channels and other independent pathways [2, 3]. To date, eight mGlus subtypes are reported and further divided into three subgroups according to sequence homology, cell signaling transduction and pharmacology [4, 5]. Group I ($mGlu_1$ and $mGlu_5$) are mainly expressed postsynaptic to activate phospholipase C or adenylyl cyclase (ACs). In general, both group II ($mGlu_2$ and $mGlu_3$) and III ($mGlu_4$ and $mGlu_{6\text{-}8}$) are located pre- and postsynaptic and have similar mechanism of action, which inhibit ACs and regulate ion channels [1, 6].

Among group III, $mGlu_7$ is widely distributed in the CNS. The striatum, hippocampus, thalamus and neocortex are the most abundant regions with $mGlu_7$ expression. As auto- or hetero-receptors, $mGlu_7$ activation results in an attenuated release of the endogenous neurotransmitters, glutamate or gamma-aminobutyric acid (GABA) in the presynaptic regions of glutamatergic or GABAergic terminals, respectively [3, 5, 7, 8]. Several reports uncovered that $mGlu_7$ plays an important role in the processes of learning and memory [9-11]. Of note, dysregulation of $mGlu_7$ signaling can be observed under some neuropathological conditions, such as Alzheimer's disease (AD) [12], Parkinson's disease (PD) [13], Huntington's disease (HD) [14] and Rett syndrome [15]. Thus, $mGlu_7$ has been studied as a potential therapeutic target in several animal models of neurodegenerative diseases [16-20]. In addition to endogenous agonists like glutamate, several exogenous $mGlu_7$ agonists and antagonists have been found and used in $mGlu_7$ studies (**Figure 1A**, **1B**). In recent years, several allosteric $mGlu_7$ modulators, both positive and negative, have attracted more attention and some progress has been made owing to their high selectivity and reduced side effects (shown in **Figure 1C**, **1D**) [6, 7, 21,

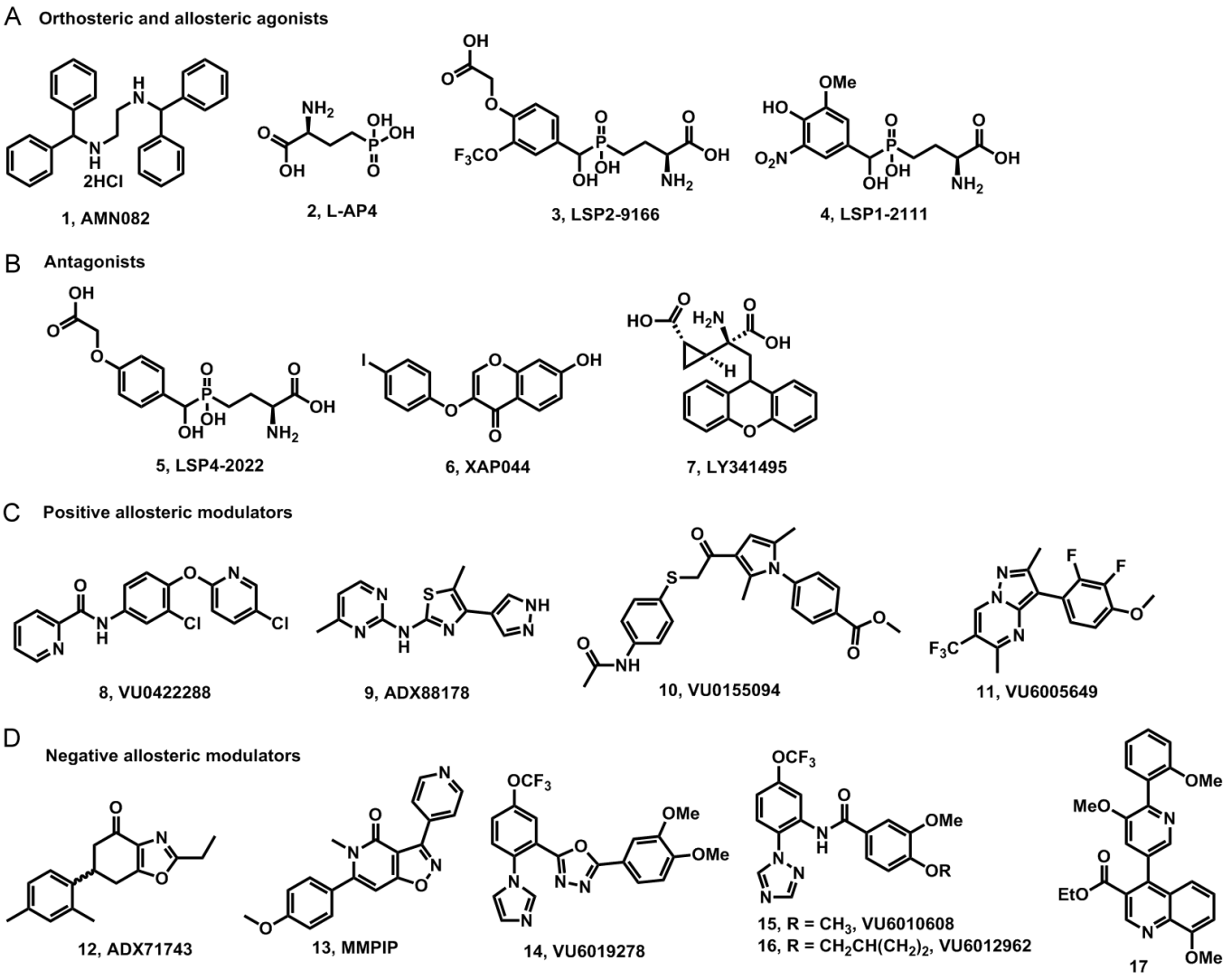

Figure 1. Representative mGlu$_7$ modulators.

22]. However, these molecules have not been used as clinical drugs for reasons including low subtype-selectivity, poor bioavailability and inability to cross the blood-brain barrier (BBB).

Positron emission tomography (PET) is a highly sensitive imaging technology for pre-clinical and clinical functional molecular imaging. After the appropriate radiolabeled ligand is injected in a non-pharmacological dose, three-dimensional images, including the concentration and location information of the radioligand, could be obtained to reveal the physiological state of the target through non-invasive data collection and reconstruction [23-25]. Although the development of mGlu$_7$-selective PET tracers will contribute to the mechanism study of mGlu$_7$-associated disease and drug discovery, only one PET tracer derived from mGlu$_7$ negative allosteric modulator (NAM), [^{11}C]MMPIP was developed and evaluated in rodents. Due to its moderate affinity to mGlu$_7$ (26 nM) [26] and the existing radioactive metabolites in the brain, [^{11}C]MMPIP cannot be used for the quantitative assessment of mGlu$_7$ [27]. Therefore, compound 18 (MG7-2109) (**Figure 2**) [26], with improved affinity to mGlu$_7$ (reported IC_{50} = 12 nM) was selected as a candidate compound in this work. Radiosynthesis of [^{11}C]18 followed by *in vitro* autoradiography, *ex vivo* biodistribution and PET studies on rodent brains were conducted to assess its performance for imaging mGlu$_7$ in the brain.

Materials and methods

General

Unless otherwise stated, reagents, solvents, and chemicals were purchased from commercially available vendors and used without further purification. The chemical synthesis of compound 18 (MG7-2109) and corresponding precursor 19 were synthesized according to the previous report [26]. Nuclear magnetic resonance (NMR) spectra were recorded in an AVANCE NEO 400MHZ spectrometer. ^{1}H NMR chemical shifts (δ) are reported in parts per million (ppm) relative to TMS with the residual solvent peak

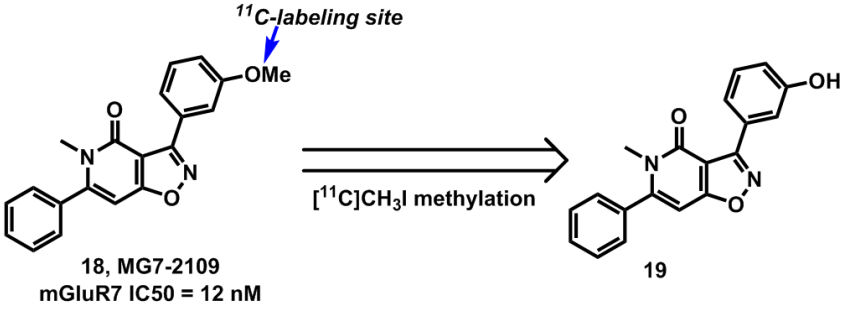

Figure 2. Proposed mGlu$_7$-selective PET radioligand and the responding precursor.

used as an internal reference. Abbreviations used are singlet (s), doublet (d), triplet (t), quartet (q), and multiplet (m). High-performance liquid chromatography-mass spectrometry (HPLC-MS) was performed on Shimadzu LCMS-2010EV single four-stage rod mass spectrometer ESI electric spray ion source or Agilent single four-stage rod 6120B ESI electric spray ion source.

Chemistry

(E)-3-methoxybenzaldehyde oxime 21: A solution of 3-methoxybenzaldehyde 20 (5.0 g, 36.8 mmol) and TEA (5.6 g, 55.1 mmol) and hydroxylamine hydrochloride (3.8 g, 55.1 mmol) in EtOH/H_2O (50 mL/50 mL) was stirred at room temperature overnight. Then the reaction was extracted with water and EtOAc. The organic phase was washed brine, then dried on Na_2SO_4 and concentrated in vacuum. The residue was purified by silica gel column (petroleum ether/EtOAc = 8/1) to give (*E*)-3-methoxybenzaldehyde oxime 21 (6.0 g, yield 90%) as a colorless oil.

(Z)-N-hydroxy-3-methoxybenzimidoyl chloride 22: To a solution of (*E*)-3-methoxybenzaldehyde oxime 21 (3.7 g, 24.5 mmol) in DMF (50 mL) was added NCS (2.9 g, 22 mmol) in batches at 0°C. Then the solution was stirred at 0°C to room temperature overnight. The solution was extracted with water and EtOAc. The EtOAc phase was washed with brine, dried over Na_2SO_4 and concentrated in vacuum to give (*Z*)-N-hydroxy-3-methoxybenzimidoyl chloride 22 (3.7 g, yield 82%) as a colorless oil without further purification.

(Z)-3-(pyrrolidin-1-yl)but-2-enoate 24: A solution of pyrrolidine (2.5 g, 35.0 mmol) and ethyl 3-oxobutanoate 23 (4.7 g, 35.5 mmol) in toluene (25 mL) was stirred at 115°C for 2 h with Dean-stark. Then the solution was concentrated in vacuum to give ethyl (*Z*)-3-(pyrrolidin-1-yl)but-2-enoate 24 (6.0 g, yield 71%) as a yellow oil for next step without further purification.

ethyl 3-(3-methoxyphenyl)-5-methylisoxazole-4-carboxylate 25: To a solution of ethyl (Z)-3-(pyrrolidin-1-yl)but-2-enoate 24 (6.0 g, 33.0 mmol) and TEA (6.0 g, 60.0 mmol) in DCM (40 mL) was added dropwise (*Z*)-N-hydroxy-3-methoxybenzimidoyl chloride 22 (3.7 g, 20.0 mmol) in DCM (40 mL) at 0°C. Then the solution was stirred at room temperature overnight. The solution was diluted with DCM, washed with *1N* HCl and brine successively, dried over Na_2SO_4 and concentrated in vacuum. The residue was purified by silica gel column (petroleum ether/EtOAc = 2/1) to give 1.8 g crude and then purified by reversed-phase column (MeOH = 0-95%) to give ethyl 3-(3-methoxyphenyl)-5-methylisoxazole-4-carboxylate 25 (350.0 mg, yield 6%) as a yellow oil. ^{1}H NMR (400 MHz, DMSO-d_6) δ 7.42 - 7.38 (m, 1H), 7.17 - 7.15 (m, 2H), 7.11 - 7.08 (m, 1H), 4.18 (q, *J* = 8.0 Hz, 2H), 3.80 (s, 1H), 2.71 (s, 3H), 1.16 (t, *J* = 8.0 Hz, 3H).

3-(3-methoxyphenyl)-N,5-dimethylisoxazole-4-carboxamide 26: A solution of ethyl 3-(3-methoxyphenyl)-5-methylisoxazole-4-carboxylate 25 (550.0 mg, 2.1 mmol) and methylamine/MeOH (10 mL) in sealed tube was stirred at 85°C overnight. The solution was concentrated in vacuum to give 3-(3-methoxyphenyl)-N,5-dimethylisoxazole-4-carboxamide 26 (500.0 mg, yield 96%) as a light-yellow solid. ^{1}H NMR (400 MHz, DMSO-d_6) δ 8.31 (brs, 1H), 7.43 - 7.39 (m, 1H), 7.25 - 7.23 (m, 2H), 7.09 - 7.07 (m, 1H), 3.80 (s, 3H), 2.74 (s, 3H), 2.53 (s, 3H).

3-(3-methoxyphenyl)-N-methyl-5-(2-oxo-2-phenylethyl)isoxazole-4-carboxamide 27: To a solution of 3-(3-methoxyphenyl)-N,5-dimethylisoxazole-4-carboxamide 26 (250.0 mg, 1.0 mmol) in dry THF (40 mL) n-BuLi (1.0 mL, 2.5 M/L, 2.2 mmol) was added dropwise at -70°C under N_2. Then the solution was stirred at -70°C for 1.5 h. Then methyl benzoate 7 (305.0 mg, 2.2 mmol) in dry THF (1 mL) was added dropwise at -65°C and the solution was stirred at this temperature for 1.5 h. Then the solution was stirred at room temperature. The solution was poured into ice water and extracted with water and EtOAc. The EtOAc phase was washed with brine, dried over Na_2SO_4 and concentrated in vacuum. The residue was purified by flash (petroleum ether/EtOAc = 2/1) to give 3-(3-methoxyphenyl)-N-methyl-5-(2-oxo-2-phenylethyl)isoxazole-4-carboxamide 27 (160 mg, yield 45%) as a light yellow oil.

3-(3-methoxyphenyl)-5-methyl-6-phenylisoxazolo[4,5-c]pyridin-4(5H)-one (18): To a solution of 3-(3-methoxyphenyl)-N-methyl-5-(2-oxo-2-phenylethyl)isoxazole-4-carboxamide 27 (160.0 mg, 0.4 mmol) in toluene (8 mL), *p*-Toluenesulfonic acid monohydrate (86.0 mg, 0.4 mmol) was added, then the solution was stirred at 110°C overnight. The solution was diluted with EtOAc. The EtOAc phase was washed with saturated Na_2CO_3 and brine, dried over Na_2SO_4 and concentrated in vacuum to give 3-(3-methoxyphenyl)-5-methyl-6-phenylisoxazolo[4,5-c]pyridin-4(5H)-one 18 (120.0 mg, yield 79%) as a brown solid. ^{1}H NMR (400 MHz, Chloroform-d_3) δ 7.99 - 7.91 (m,

2H), 7.55 - 7.50 (m, 3H), 7.45 - 7.38 (m, 3H), 7.06 (ddd, *J* = 8.3, 2.7, 1.0 Hz, 1H), 6.54 (s, 1H), 3.91 (s, 3H), 3.42 (s, 3H). Purity: 97%. HPLC-MS, m/z = 333.0 (M + 1).

3-(3-hydroxyphenyl)-5-methyl-6-phenylisoxazolo[4,5-c] pyridin-4(5H)-one (19): To a solution of 3-(3-methoxyphenyl)-5-methyl-6-phenylisoxazolo[4,5-c]pyridin-4(5H)-one 18 (100.0 mg, 0.3 mmol) in dry DCM (20 mL) was added BBr_3 (0.3 mL) at 0°C, then the solution was stirred at 0°C for 20 min and then warmed to room temperature stirred for 7 h. The solution was diluted with DCM and poured into ice water. The DCM phase was washed with brine, dried over Na_2SO_4 and concentrated in vacuum. The residue was purified by reversed-phase column chromatography (MeOH = 0-95%) to give 3-(3-hydroxyphenyl)-5-methyl-6-phenylisoxazolo[4,5-c]pyridin-4(5H)-one 19 (40.0 mg, yield 42%) as a white solid. ^{1}H NMR (400 MHz, Chloroform-d_3) δ 7.95 - 7.89 (m, 1H), 7.79 (dt, *J* = 7.9, 1.2 Hz, 1H), 7.52 (dt, *J* = 4.4, 2.9 Hz, 3H), 7.44 - 7.32 (m, 3H), 7.00 (ddd, *J* = 8.2, 2.7, 1.0 Hz, 1H), 6.57 (s, 1H), 3.40 (s, 3H). Purity: 97%. HPLC-MS, m/z = 319.1 (M + 1).

Pharmacology

Cell line generation: In order to generate human mGlu$_7$ stable cell lines to be used for thallium flux assays, human mGlu$_{7A}$ was prepared by PCR amplification (from plasmid GRM70000001 from the cDNA Resource Center) of the entire coding sequence of each receptor and cloning into pIRES puro 3 (Invitrogen). The cloning sites were NheI/NotI. HEK GIRK cells, generously provided by Lily Jan (University of California San Francisco, San Francisco, CA), were transfected with 24 μg of DNA using Fugene6 (Promega), stable transfectants were selected with 1000 ng/mLpuromycin dihydrochloride (Sigma-Aldrich, St. Louis, MO), and polyclonal human mGlu$_7$ GIRK cell lines were established. Cells were maintained following selection in 45% DMEM, 45% Ham's F12, 10% FBS, 100 units/mL penicillin/streptomycin, 20 mM HEPES, pH 7.3, 1 mM sodium pyruvate, 2 mM glutamine, 700 μg/mL G418 (Mediatech, Inc., Herndon, VA), and 600 μg/mL puromycin (growth media) at 37°C in the presence of 5% CO_2. All cell culture reagents were purchased from Invitrogen Corp. (Carlsbad, CA) unless otherwise noted.

Human mGlu$_7$ thallium flux in vitro assays: Compound activity at mGlu$_7$ was assessed using thallium flux through GIRK channels, a method that has been previously described in detail [28]. For Schild analysis experiments a full concentration-response of L-AP4 was utilized in the absence and presence of fixed concentrations of MG7-2109. For potency evaluation experiments an EC_{80} concentration of L-AP4 was utilized. Data were analyzed using Excel (Microsoft Corp, Redmond, WA). The slope of the fluorescence increase beginning 5 s after thallium/agonist addition and ending 15 s after thallium/agonist addition was calculated, corrected to vehicle and maximal L-AP4 control slope values, and plotted using either XLfit (ID Business Solutions Ltd.) or Prism software (GraphPad Software, San Diego, CA) to generate concentration-response curves. Potencies were calculated from fits using a four-point parameter logistic equation.

Radiochemistry

[^{11}C]CH_3I was prepared from [^{11}C]CO_2 in cyclotron and then transferred into a precooled reaction vial (-15 to -20°C) containing the precursor 19 (0.95 mg), NaOH (0.5 *M*, 6.3 μL), and DMF (300 μL). After the transfer, this reaction mixture was heated at 80°C for 5 min. Then HPLC buffer (CH_3CN/H_2O = 70/30, 0.1% Et_3N, 0.5 mL) was added and then injected into HPLC for purification (column: CAPCELL PAK UG80 C18 column, 10 mm ID × 250 mm; buffer: CH_3CN/H_2O (70/30, 0.1% Et_3N); flow rate: 5.0 mL/min). [^{11}C]18 was obtained in 23 ± 4% radiochemical yield (decay-corrected, n = 5) at the end of synthesis (EOS) based on [^{11}C]CO_2. [^{11}C]18 was generated with excellent radiochemical purity (> 99%) and molar activity (201 ± 111 GBq/μmol, n = 5).

In vitro stability and protein binding

In vitro serum stability: 400 μL of mouse, rat, non-human primate, and human serum were preincubated at 37°C for 5 min. Subsequently, [^{11}C]18 (approximately 1.5 mCi) was added to the samples and incubated at 37°C for 30 min, followed by the addition of 400 μL ice-cold MeCN to terminate the enzymatic reactions, as well as vortexing and centrifuging at 10,000×g for 5 min. The percentage of intact parent and radiometabolites was assessed by radio-HPLC using buffer CH_3CN/H_2O (70/30, 0.1% Et_3N). As a negative control, the same experiment is carried out with PBS instead of serum.

Plasma protein binding: The plasma protein binding was conducted according to a previous report [29]. Briefly, 1.5 mCi of [^{11}C]18 was added per 150 μL of plasma that has been preincubated under 37°C for 5 min. The samples were incubated at room temperature for 10 min. To each 150 μL of radiotracer-plasma solution was added 300 μL of ice-cold PBS and all samples were briefly vortexed. 300 μL of each sample was added into the filters with a size cutoff of 10 kDa, and the samples were centrifuged at 21000 g for 15 min at 4°C. The filters were then washed with 300 μL PBS at 21000 g for 20 min at 4°C; 300 μL cold PBS was used to wash the tube and collect all the filtrates to obtain the protein fraction. The radioactivity of the protein fraction and filtrate was measured in a gamma counter (Wizard, PerkinElmer), and the free fraction f_u was calculated according to the following equation:

$$f_u = 1 - (A_{protein}/A_{total})$$

In vitro autoradiography

In brief, the rat brain sections (20 μm) were preincubated with Tris-HCl buffer (50 mM) at room temperature for 20 min, followed by incubation with [^{11}C]18 (1 μCi/mL) for 30 min. For blocking studies, compound 18 (1 μM) or MMPIP

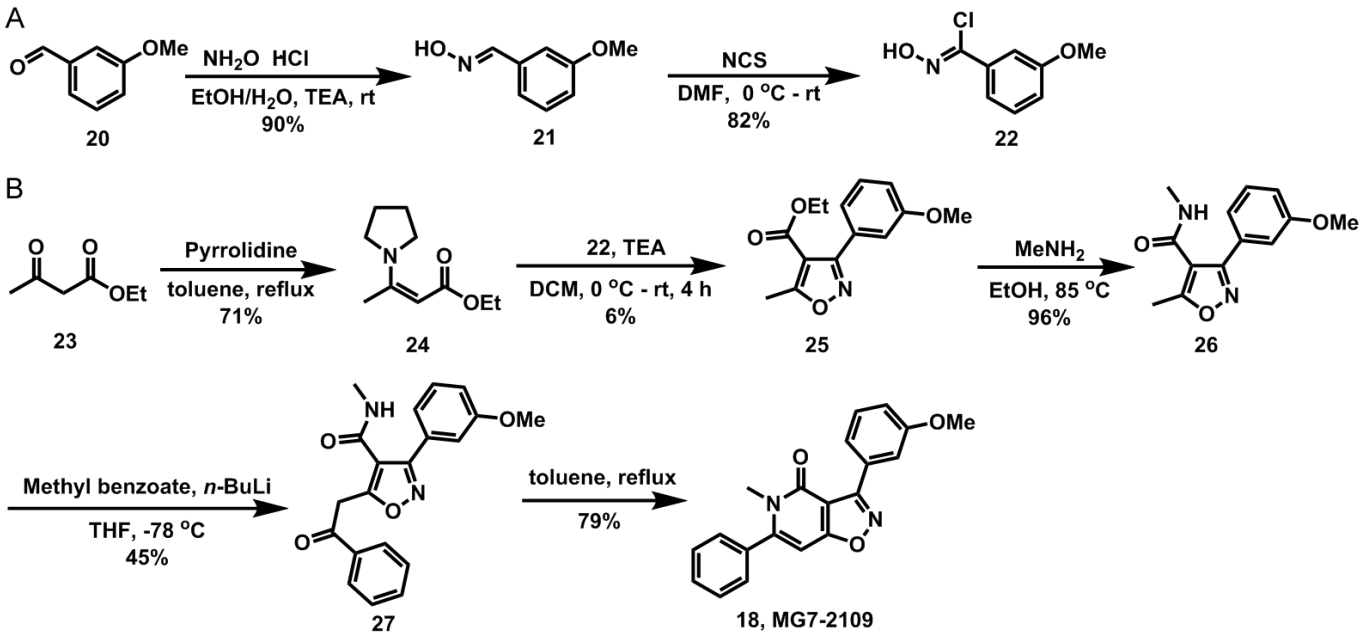

Figure 3. Chemical synthesis of 18 (MG7-2109).

(1 μM) was added to the incubation solution. Then the brain sections were washed with an ice-cold thrice for 2 min and dipped in cold distilled water for 10 s. Subsequently, the brain slices were dried and positioned on imaging screens (BAS-MS2025, GE Healthcare, USA). Then the screen was scanned by an Amersham Typhoon 5 analyzer system. The radioactivity values were normalized as a percentage of the radioactivity relative to the control.

PET imaging

An Inveon PET scanner (Siemens) was used for dynamic PET imaging studies and [^{11}C]18 (*ca*. 1.1 mCi/0.2 mL) was intravenously injected via the tail vein via a pre-installed catheter, and dynamic PET images were acquired in a 3D mode for a period of 60 min. The dynamic PET images were reconstructed using ASIPro VW software, and volumes of interest were calculated.

Whole-body distribution

In brief, [^{11}C]18 (50 μCi/0.1 mL) was injected intravenously into each mouse via the tail vein. At the time point of 5, 15, 30 and 60 min, mice were sacrificed by cervical dislocation and the tissues of interest were collected and weighted. An automatic gamma counter (PerkinElmer, USA) was used for determining each organ's decay-corrected radioactivity.

Results

Chemistry

The synthesis of 18 (MG7-2109) was started from the formation of oxime 21 from 3-methoxybenzaldehyde 20, followed by chlorination of obtained 21 to afford intermediate 22 in 82% yield (**Figure 3A**). On the other hand, condensation of ethyl acetoacetate 23 with pyrrolidine afforded enamine 24 in 71% yield. Cycloaddition of oxime 22 and enamine 24 delivered isoxazole 25 in 6% yield. Ammonolysis of 25 with methylamine provided amide 26 in 96% yield, which reacted with methyl benzoate to give intermediate 27 in the presence of excess *n*-BuLi at -78°C. Cyclization of ketone 27 in boiling toluene afforded the "cold" isoxazolopyridone derivative 18 (MG7-2109) in 79% yield (**Figure 3B**).

Pharmacology

As shown in **Figure 4A**, MG7-2109 (30 μM, 10 μM, 3333 nM, 1111 nM, 370 nM, 123 nM, or 41 nM), dose-dependently decreased the maximal response of L-AP4 (a group III-selective mGlu agonist) toward mGlu$_7$ in the G protein-coupled inwardly rectifying potassium (GIRK) thallium assay, consistent with a noncompetitive mechanism of action. The potencies (IC_{50}s) for inhibiting an EC_{80} L-AP4 response in the mGlu$_7$ GIRK assay for MG7-2109 and MMPIP were evaluated using the mGlu$_7$ NAM XAP044 as a positive control. The results revealed MG7-2109 and MMPIP exhibit NAM activity with IC_{50} values of 81 nM and 223 nM, respectively, while the positive control XAP044 displayed a potency of 162 nM in the human mGlu$_7$ GIRK assay (**Figure 4B**). Pharmacokinetic parameters of MG7-2109 in Sprague Dawley (SD) rats appeared rapid metabolic clearance in blood and brain after a single intravenous administration (**Figure 4C**). The off-target screening of MG7-2109 to numerous classical targets in CNS including receptors, transporters and ion channels was conducted. No significant off-target binding of MG7-2109 was observed towards 59 CNS targets (< 50% inhibition) at

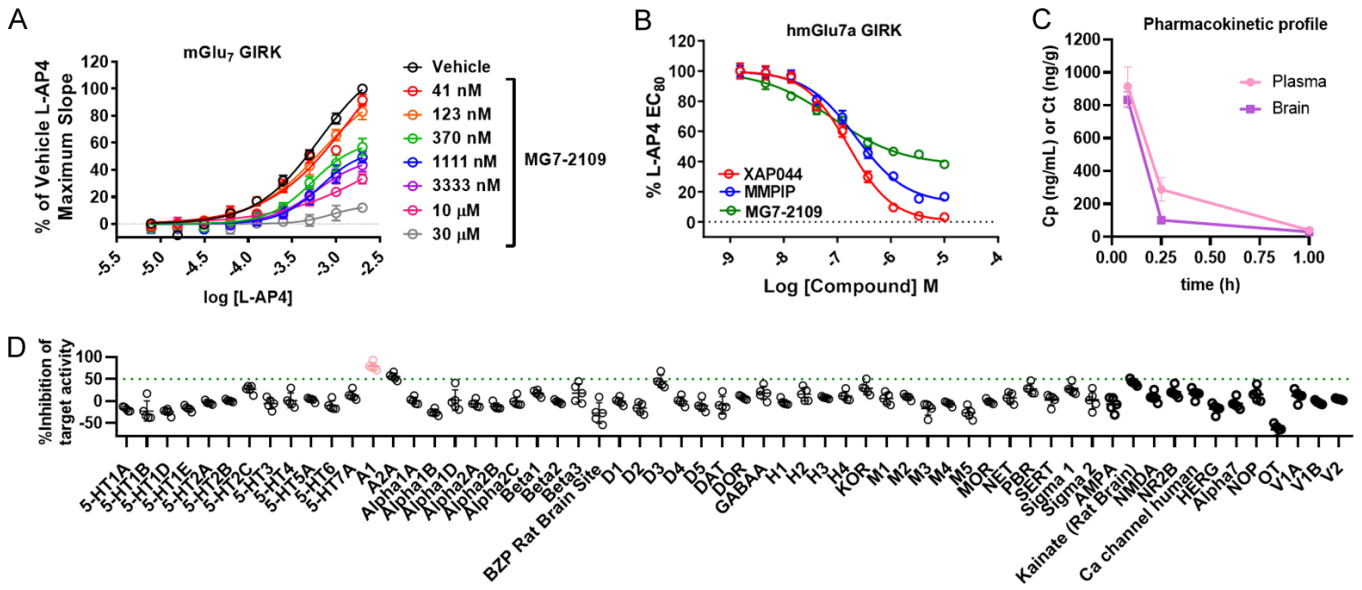

E

Parameters	MG7-2109
MW[a]	332.36
clogP[a]	4.21
logD	3.39
tPSA[a]	51.13
MPO score[b]	5.5

mGluRs family	Agonist IC_{50} (μM)	Antagonist IC_{50} (μM)
$mGluR_1$	10	10
$mGluR_2$	10	1
$mGluR_3$	2	1.8
$mGluR_4$	1.2	0.85
$mGluR_5$	10	10
$mGluR_6$	1	1.1
$mGluR_8$	1.1	1.1

CYP isoforms	% Enzyme Activity at 5 μM
CYP1A2	93.4
CYP2C19	102.5
CYP2C9	36.03 (IC_{50} = 3.2 μM)
CYP2D6	101.3
CYP3A4	96.8
CYP19A	104.8
hERG IC_{50}	>100 μM

Figure 4. A. MG7-2109 noncompetitively decreases the maximal L-AP4 response in mGlu$_7$ GIRK thallium flux assays. B. *In vitro* evaluation of the potencies of MG7-2109, MMPIP, and the control mGlu$_7$ antagonist XAP044 in mGlu$_7$ GIRK thallium flux assays. C. Plasma and brain concentration-time profiles of MG7-2109 following a single intravenous administration to SD rats (male, dose: 1 mg/kg). D. Off-target pharmacological evaluation of MG7-2109 against major CNS targets at a concentration of 10 μM. E. Physicochemical properties and inhibitory activity of MG7-2109. [a]Values were calculated with ChemDraw 21.0 software. [b]Values were predicted with ACD/labs.

the concentration of 10 μM, except A1 (Ki = 644 nM) (**Figure 4D**). As summarized in **Figure 4E**, the cLogP value of MG7-2109 was predicted as 4.21, and the LogD value was determined to be 3.39 through the 'shake-flask' method. The topological polar surface area (tPSA) and multiparameter optimization (MPO) score of MG7-2109 were assessed as 51.13 and 5.5, respectively. Additionally, the agonists or antagonists IC_{50} values of MG7-2109 against other members of the mGlu family were measured in the range of 0.85 μM to 10 μM. The inhibition of cytochromes P450 (CYP) enzymes was assessed by using 5 μM of MG7-2109. Weak inhibition (IC_{50} > 5 μM) was observed for 1A2, 2C19, 2D6, 3A4 and 19A isoforms, while the IC_{50} of 2C9 isoform was measured as 3.2 μM. Meanwhile, the hERG IC_{50} of MG7-2109 was determined to be > 100 μM.

Radiochemistry

As shown in **Figure 5**, demethylation of 18 using boron tribromide gave the desired phenol precursor 19 in 42% yield. The deprotonation of the hydroxyl group of precursor 19 with NaOH promoted the carbon-11 methylation reaction at 80°C for 5 min. The desired radiotracer [^{11}C]18 was obtained in 23% decay-corrected radiochemical yield (RCY) with more than 99% radiochemical purity at the end of synthesis (EOS).

In vitro formulation stability and protein binding

In vitro stability studies indicated that [^{11}C]18 has excellent stability after incubation with different species of serum (mice, rat, NHP and human) at 37°C for 30 min (**Figure 6A**). In addition, [^{11}C] MG7-2109 demonstrated lower protein binding in mice, rat and NHP plasma (> 40% free fraction), while higher protein binding of [^{11}C]MG7-2109 in human serum was observed (**Figure 6B**).

In vitro autoradiography studies

In vitro autoradiography studies of [^{11}C]18 were performed on the rat brain sections under baseline and blocking conditions. Unfortunately, the ARG results revealed nearly homogeneous radiotracer distribution under baseline conditions, and no obvious blocking effects were detected by using cold compound 18 (1 μM, self-blocking) and MMPIP (1 μM) as blocking reagents (**Figure 7**).

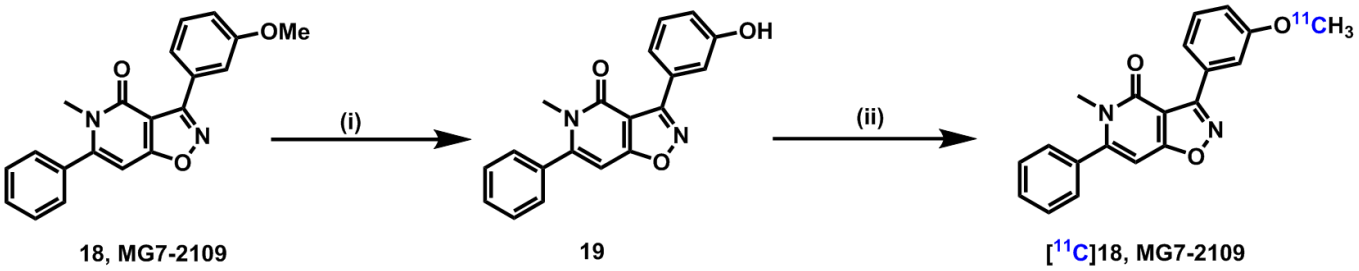

Figure 5. i. BBr_3, DCM, 0 °C, 2 h, 42%; ii. [^{11}C]CH_3I, 0.5 *M* NaOH, DMF, 80 °C, 5 min, 23% decay-corrected RCY for [^{11}C]18.

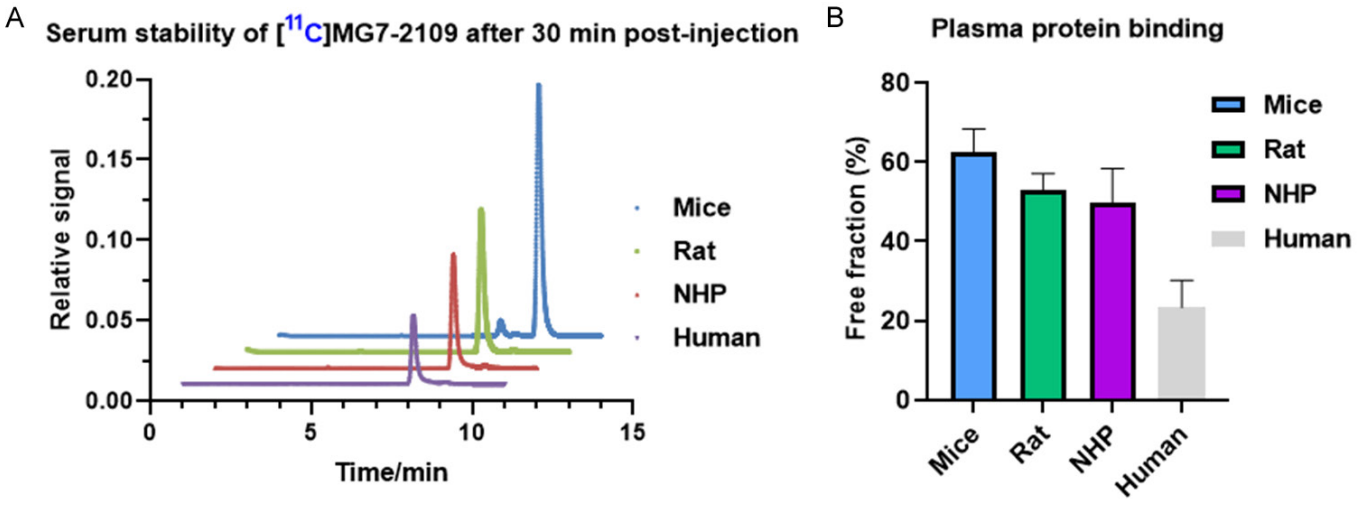

Figure 6. A. Formulation stability of [^{11}C]MG7-2109 in serum of mice, rats, NHPs, and humans at 30 min; B. Free fraction of [^{11}C]MG7-2109 in plasma, n = 3. NHP = non-human primates.

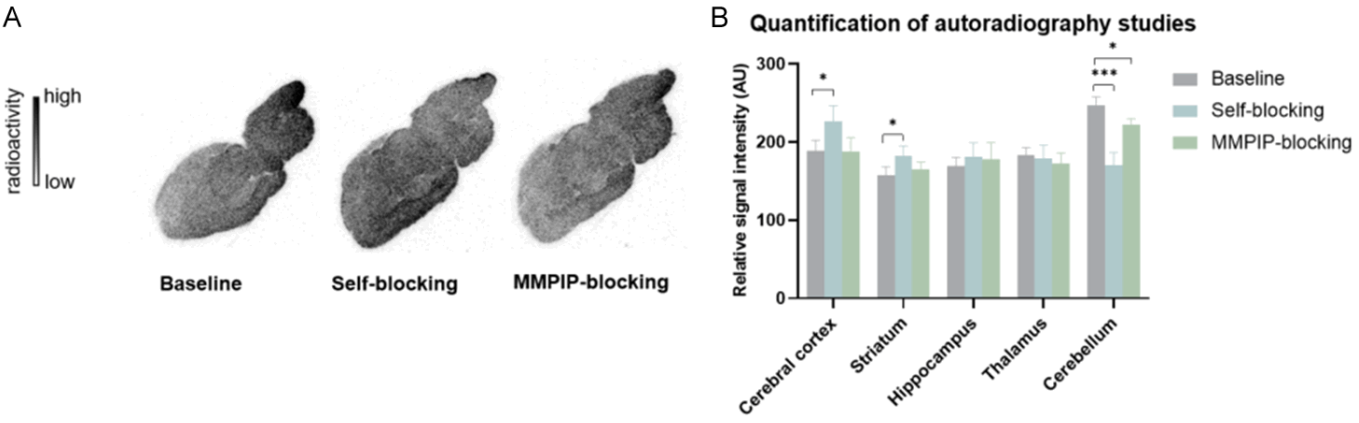

Figure 7. *In vitro* autoradiography of [^{11}C]18. A. Representative images for baseline and blocking (1 μM) autoradiography studies with [^{11}C]18. B. Quantification of autoradiography studies with [^{11}C]18. All data were referred to as mean ± SD, $n \geq 3$. Asterisks were used to indicate statistical significance: $^*P \leq 0.05$ and $^{***}P \leq 0.001$.

In vivo PET imaging study

The *in vivo* PET imaging study in rat brains was conducted and the results are illustrated in **Figure 8**. Consistent with the ARG results, a homogeneous uptake of [^{11}C]18 was observed followed by rapid clearance in rat brains.

Whole-body biodistribution study

The biodistribution study was performed in mice and the radioactivity levels of [^{11}C]18 in major organs were measured at 5-, 15-, 30- and 60-min post-tracer administration (**Figure 9**). The results showed high uptake (%ID/g >

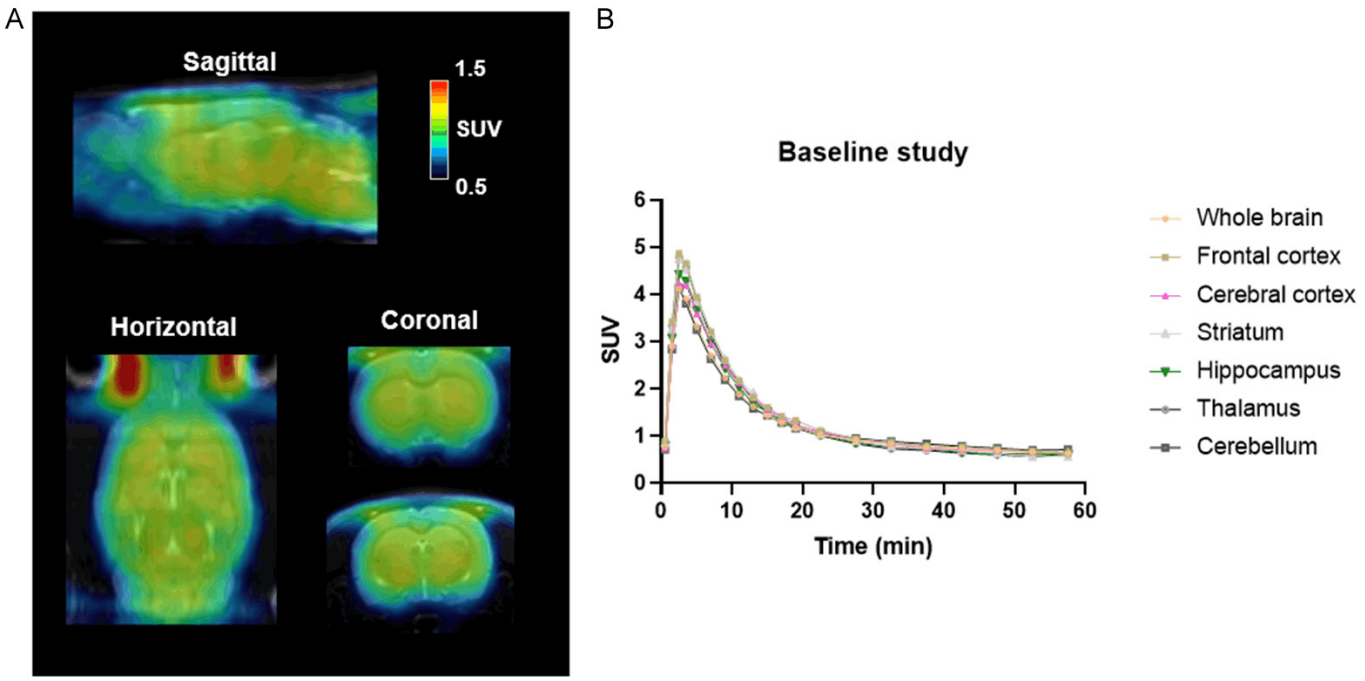

Figure 8. A. Summed PET images (5-20 min) [^{11}C]18 in rat brains under baseline conditions. B. TACs of [^{11}C]18 in various brain regions of interest.

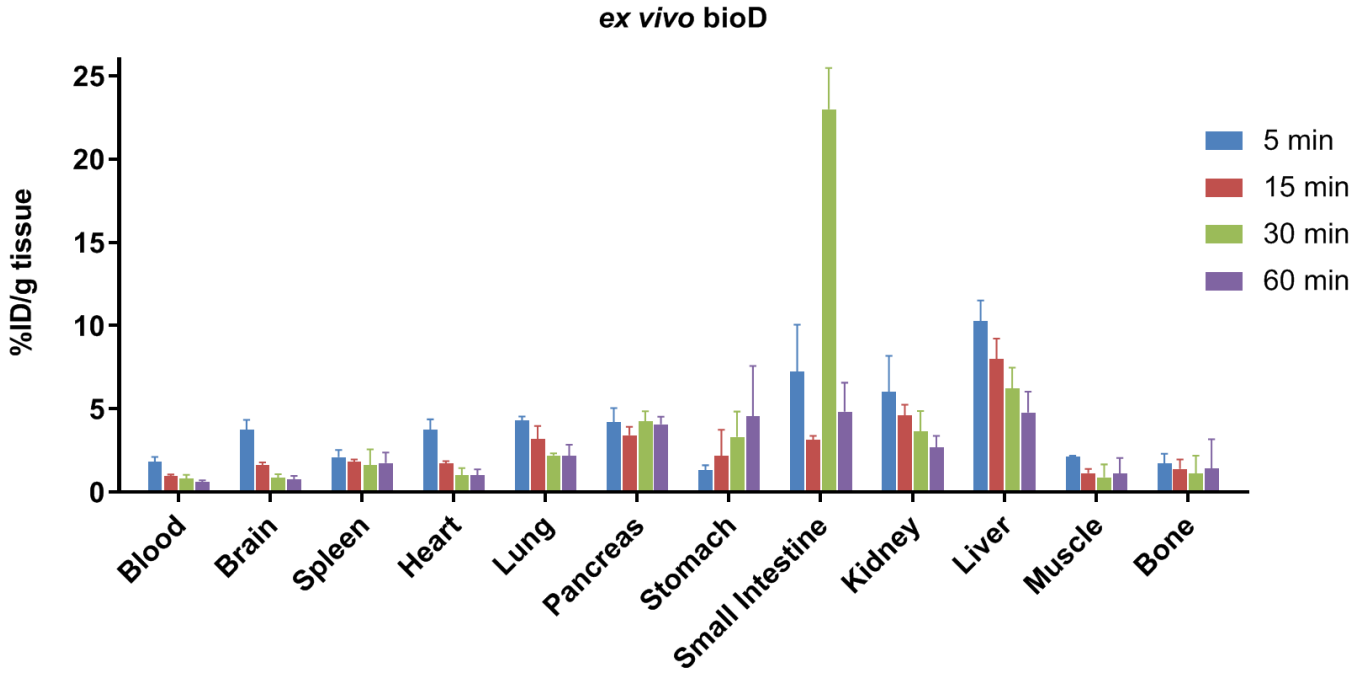

Figure 9. Whole-body *ex vivo* biodistribution studies of [^{11}C]18 in CD-1 mice. All data are referred to as mean ± SD, $n \geq 3$.

3) in the brain, heart and lung at 5 min, followed by gradual clearance in 60 min post tracer administration. The high tracer uptake in small intestine (> 20 %ID/g) and liver (> 10 %ID/g) were also detected.

Discussion

To date, [^{11}C]MMPIP is the only characterized mGlu$_7$-targeted radiotracer. Although *in vitro* ARG study demonstrated specific binding of [^{11}C]MMPIP with mGlu$_7$, PET imaging of mGlu$_7$ in the living brain was not successful due to its low affinity to mGlu$_7$. In this study, we aim to evaluate an analog of MMPIP compound 18 with improved binding activity to mGlu$_7$, for PET imaging of mGlu$_7$. The synthesis of reference compound 18 was accomplished starting from the commercially available methoxybenzaldehyde 20 through seven steps and afforded the desired product 18 (MG7-2109) in 1.5% overall yield (**Figure 3**).

Schild analysis of the activity of 18 towards a concentration response of the group III mGlu agonist L-AP4 in the human $mGlu_7$ GIRK thallium flux assay is consistent with 18 acting as an $mGlu_7$ NAM. The inhibition potency (IC_{50}) of XAP044, MMPIP and 18 against an $mGlu_7$ L-AP4 EC_{80} response was also evaluated in the $mGlu_7$ GIRK thallium flux assay. Although the IC_{50} values (MMPIP IC_{50}: 223 nM and 18 IC_{50}: 81 nM) diverged compared to the reported data (MMPIP IC_{50}: 26 nM and 18 IC_{50}: 12 nM) [30], a consistent inhibition trend was observed (**Figure 4B**). Of note, the reported IC_{50} values for MMPIP and MG7-2109 were performed in a different assay utilizing the rat $mGlu_7$ receptor (calcium mobilization assays utilizing the promiscuous G protein $G_{\alpha 15}$) than the data reported herein. The pharmacokinetics of 18 was assessed *via* a single intravenous administration to SD rats (1 mg/kg) at 0.08, 0.25- and 1-hour time point (Table S1). The brain/plasma ratio of MG7-2109 ranged between 0.36 to 0.92, indicating that 18 has sufficient CNS penetration [31]. The off-target screening against 60 enzymes, GPCRs and ion channels indicated no significant off-target activity of 18 at the concentration of 10 μM. CNS MPO score is widely used to predict the probability of a drug candidate crossing the BBB, and MPO score ≥ 4 is highly desirable. The MPO score of 18 was calculated as 5.5, suggesting it has favorable BBB penetration properties. The selectivity assay for 18 towards mGlus group I and other group II subtypes revealed that 18 is a selective compound for $mGlu_7$. The assay of CYP450s and hERG channel inhibitory properties is essential to evaluate drug toxicity and potential drug-drug interactions. The low inhibitory effect of CYP450s (IC_{50} ≥ 3.2 μM) and hERG (IC_{50} > 100 μM) demonstrated a favorable safety profile of MG7-2109.

Based on the structure of 18, the methyl group on the phenol ring is proposed as the labeling position [32, 33]. Indeed, the precursor 19 could be easily synthesized from 18 by treatment with BBr_3. The carbon-11 methylation reaction was carried out by deprotonation of the hydroxyl group of precursor 19 with NaOH, yielding the desired radiotracer [^{11}C]18 in 23% RCY. [^{11}C]18 identity was confirmed by co-injection on HPLC with the standard 18, and radiochemical purity was > 99%. *In vitro* stability tests of [^{11}C]18 were performed in mice, rat, NHP and human serum, and then analyzed by radio-HPLC to determine the fraction of parent tracer. To investigate the efficacy and toxicity of [^{11}C]18, free drug concentrations in different types of plasma were measured by serum protein binding and fraction unbound (fu). While fewer differences in protein binding affinity were observed for mice, rat, and NHP, lower fu value of [^{11}C]18 in human plasma were detected. *In vitro* ARG studies using rat brain sections were conducted to assess the specific binding of [^{11}C]18. Under baseline conditions, the highest radioactivity was found in the cerebellum. Other regions like cortex and thalamus had relatively lower levels of tracer uptake. However, blocking studies with excess 18 and MMPIP did not significantly reduce the radioactive signals, indicating limited specific binding of [^{11}C]18 with $mGlu_7$. *In vivo* PET imaging study in the rat brain revealed a homogeneous distribution of [^{11}C]18 and rapid clearance, which was in accordance with limited specific binding observed in ARG results. The biodistribution study in mice was performed to assess the radioactivity distribution in different tissues/organs. High radioactivity was detected in the small intestine, liver, and kidney, which indicated that [^{11}C]18 may be excreted through the hepatobiliary and urinary system.

Conclusion

In this work, a novel carbon-11 labeled radiotracer [^{11}C]18 (MG7-2109) was synthesized *via* ^{11}C-methylation in 23% decay-corrected RCY. Comprehensive *in vitro* stability, protein binding, autoradiography, and *ex vivo* biodistribution studies were conducted to evaluate the performance characteristics of [^{11}C]18 for specific binding to $mGlu_7$. Although this tracer was not successful for PET imaging of $mGlu_7$, this study offers valuable insights for developing $mGlu_7$-targeted radiotracer based on the isoxazolo(5,4-c) pyridine scaffold.

Acknowledgements

We thank the Division of Nuclear Medicine and Molecular Imaging, Radiology, MGH and Harvard Medical School, and Department of Radiology and Imaging Sciences, Emory University School of Medicine for general support. This research was partly funded by Grant-in-Aid for Scientific Research (KAKENHI) No. B-23H02867 from the Japanese Ministry of Education, Culture, Sports, Science and Technology and Moonshot Research and Development Program No. 21zf0127003h001 from Japan Agency for Medical Research and Development.

Disclosure of conflict of interest

None.

Address correspondence to: Ming-Rong Zhang, Department of Advanced Nuclear Medicine Sciences, Institute for Quantum Medical Sciences, National Institutes for Quantum Science and Technology, Chiba 263-8555, Japan. E-mail: zhang.ming-rong@qst.go.jp; Steven H Liang, Department of Radiology and Imaging Sciences, Emory University, Atlanta, GA 30322, USA. E-mail: steven.liang@emory.edu

References

[1] Waxham MN. Chapter 10 - neurotransmitter receptors. In: Byrne JH, Heidelberger R, Waxham MN, editors. From Molecules to Networks. 3rd Edition. Boston: Academic Press; 2014. pp. 285-321.

[2] Ribeiro FM, Vieira LB, Pires RG, Olmo RP and Ferguson SS. Metabotropic glutamate receptors and neurodegenerative diseases. Pharmacol Res 2017; 115: 179-91.

[3] Niswender CM and Conn PJ. Metabotropic glutamate receptors: physiology, pharmacology, and disease. Annu Rev Pharmacol Toxicol 2010; 50: 295-322.

[4] Traynelis SF, Wollmuth LP, McBain CJ, Menniti FS, Vance KM, Ogden KK, Hansen KB, Yuan H, Myers SJ and Dingledine R. Glutamate receptor ion channels: structure, regulation, and function. Pharmacol Rev 2010; 62: 405-96.
[5] Kew JN and Kemp JA. Ionotropic and metabotropic glutamate receptor structure and pharmacology. Psychopharmacology (Berl) 2005; 179: 4-29.
[6] Lindsley CW, Emmitte KA, Hopkins CR, Bridges TM, Gregory KJ, Niswender CM and Conn PJ. Practical strategies and concepts in GPCR allosteric modulator discovery: recent advances with metabotropic glutamate receptors. Chem Rev 2016; 116: 6707-41.
[7] Amalric M, Lopez S, Goudet C, Fisone G, Battaglia G, Nicoletti F, Pin JP and Acher FC. Group III and subtype 4 metabotropic glutamate receptor agonists: discovery and pathophysiological applications in Parkinson's disease. Neuropharmacology 2013; 66: 53-64.
[8] Dev KK, Nakanishi S and Henley JM. Regulation of mglu(7) receptors by proteins that interact with the intracellular C-terminus. Trends Pharmacol Sci 2001; 22: 355-61.
[9] Riedel G, Wetzel W and Reymann KG. (R,S)-α-Methyl-4-carboxyphenylglycine (MCPG) blocks spatial learning in rats and long-term potentiation in the dentate gyrus in vivo. Neurosci Lett 1994; 167: 141-4.
[10] Hölscher C, McGlinchey L and Rowan MJ. l-AP4 (l-(+)-2-amino-4-phosphonobutyric acid) induced impairment of spatial learning in the rat is antagonized by MAP4 ((S)-2-amino-2-methyl-4-phosphonobutanoic acid). Behav Brain Res 1996; 81: 69-79.
[11] Hölscher C, Gigg J and O'Mara SM. Metabotropic glutamate receptor activation and blockade: their role in long-term potentiation, learning and neurotoxicity. Neurosci Biobehav Rev 1999; 23: 399-410.
[12] Gu Z, Cheng J, Zhong P, Qin L, Liu W and Yan Z. Aβ selectively impairs mGluR7 modulation of NMDA signaling in basal forebrain cholinergic neurons: implication in Alzheimer's disease. J Neurosci 2014; 34: 13614.
[13] Litim N, Morissette M and Di Paolo T. Metabotropic glutamate receptors as therapeutic targets in Parkinson's disease: an update from the last 5 years of research. Neuropharmacology 2017; 115: 166-79.
[14] Li SH, Colson TL, Abd-Elrahman KS and Ferguson SSG. Metabotropic glutamate receptor 2/3 activation improves motor performance and reduces pathology in heterozygous zQ175 huntington disease mice. J Pharmacol Exp Ther 2021; 379: 74-84.
[15] Gogliotti RG, Senter RK, Fisher NM, Adams J, Zamorano R, Walker AG, Blobaum AL, Engers DW, Hopkins CR, Daniels JS, Jones CK, Lindsley CW, Xiang Z, Conn PJ and Niswender CM. mGlu$_7$ potentiation rescues cognitive, social, and respiratory phenotypes in a mouse model of Rett syndrome. Sci Transl Med 2017; 9: eaai7459.
[16] Fisher NM, Seto M, Lindsley CW and Niswender CM. Metabotropic glutamate receptor 7: a new therapeutic target in neurodevelopmental disorders. Front Mol Neurosci 2018; 11: 387.
[17] Palazzo E, Marabese I, de Novellis V, Rossi F and Maione S. Metabotropic glutamate receptor 7: from synaptic function to therapeutic implications. Curr Neuropharmacol 2016; 14: 504-13.
[18] Li X and Markou A. Metabotropic glutamate receptor 7 (mGluR7) as a target for the treatment of psychostimulant dependence. CNS Neurol Disord Drug Targets 2015; 14: 738-44.
[19] O'Connor RM, Finger BC, Flor PJ and Cryan JF. Metabotropic glutamate receptor 7: at the interface of cognition and emotion. Eur J Pharmacol 2010; 639: 123-31.
[20] Lavreysen H and Dautzenberg FM. Therapeutic potential of group III metabotropic glutamate receptors. Curr Med Chem 2008; 15: 671-84.
[21] Stansley BJ and Conn PJ. Neuropharmacological insight from allosteric modulation of mGlu receptors. Trends Pharmacol Sci 2019; 40: 240-52.
[22] Gregory KJ, Dong EN, Meiler J and Conn PJ. Allosteric modulation of metabotropic glutamate receptors: structural insights and therapeutic potential. Neuropharmacology 2011; 60: 66-81.
[23] Ametamey SM, Honer M and Schubiger PA. Molecular imaging with PET. Chem Rev 2008; 108: 1501-1516.
[24] Jones T and Townsend D. History and future technical innovation in positron emission tomography. J Med Imaging (Bellingham) 2017; 4: 011013.
[25] Berg E and Cherry SR. Innovations in instrumentation for positron emission tomography. Semin Nucl Med 2018; 48: 311-31.
[26] Nakamura M, Kurihara H, Suzuki G, Mitsuya M, Ohkubo M and Ohta H. Isoxazolopyridone derivatives as allosteric metabotropic glutamate receptor 7 antagonists. Bioorg Med Chem Lett 2010; 20: 726-9.
[27] Yamasaki T, Kumata K, Yui J, Fujinaga M, Furutsuka K, Hatori A, Xie L, Ogawa M, Nengaki N, Kawamura K and Zhang MR. Synthesis and evaluation of [11C]MMPIP as a potential radioligand for imaging of metabotropic glutamate 7 receptor in the brain. EJNMMI Res 2013; 3: 54.
[28] Dhanya RP, Sheffler DJ, Dahl R, Davis M, Lee PS, Yang L, Nickols HH, Cho HP, Smith LH, D'Souza MS, Conn PJ, Der-Avakian A, Markou A and Cosford ND. Design and synthesis of systemically active metabotropic glutamate subtype-2 and -3 (mGlu2/3) receptor positive allosteric modulators (PAMs): pharmacological characterization and assessment in a rat model of cocaine dependence. J Med Chem 2014; 57: 4154-72.
[29] Taddio MF, Mu L, Castro Jaramillo CA, Bollmann T, Schmid DM, Muskalla LP, Gruene T, Chiotellis A, Ametamey SM, Schibli R and Krämer SD. Synthesis and structure-affinity relationship of small molecules for imaging human CD80 by positron emission tomography. J Med Chem 2019; 62: 8090-100.
[30] Suzuki G, Tsukamoto N, Fushiki H, Kawagishi A, Nakamura M, Kurihara H, Mitsuya M, Ohkubo M and Ohta H. In vitro pharmacological characterization of novel isoxazolopyridone derivatives as allosteric metabotropic glutamate receptor 7 antagonists. J Pharmacol Exp Ther 2007; 323: 147-56.
[31] Hitchcock SA and Pennington LD. Structure-brain exposure relationships. J Med Chem 2006; 49: 7559-83.
[32] Deng X, Rong J, Wang L, Vasdev N, Zhang L, Josephson L and Liang SH. Chemistry for positron emission tomography: recent advances in 11C-, 18F-, 13N-, and 15O-labeling reactions. Angew Chem Int Ed Engl 2019; 58: 2580-605.
[33] Rong J, Haider A, Jeppesen TE, Josephson L and Liang SH. Radiochemistry for positron emission tomography. Nat Commun 2023; 14: 3257.

Table S1. Individual plasma and brain concentrations and brain-Kp of 18 (MG7-2109) in male Sprague Dawley rats following a single intravenous administration (Dose: 1 mg/kg)

Time (hr)	Animal ID	Plasma concentration (ng/mL)	Brain concentration (ng/g)	Brain-Kp
0.08	1	1022.78	796.77	0.78
	2	935.73	887.16	0.95
	3	786.46	820.23	1.04
	Mean	914.99	834.72	0.92
	SD	119.52	46.90	0.13
	%CV	13	6	14
0.25	4	206.01	89.10	0.43
	5	333.68	88.98	0.27
	6	324.91	125.07	0.38
	Mean	288.20	101.05	0.36
	SD	71.31	20.80	0.09
	%CV	25	21	24
1	7	39.85	28.59	0.72
	8	57.77	40.98	0.71
	9	22.59	22.50	1.00
	Mean	40.07	30.69	0.81
	SD	17.59	9.42	0.16
	%CV	44	31	20

LLOQ: 2.02 ng/mL for plasma and 1.01 ng/mL for brain.